

La_{1-x}Ag_xFeO₃/halloysites nanocomposite with enhanced visible light photocatalytic performance

Xiazhang Li^{1,2} · Wei Zhu¹ · Yu Yin¹ · Xiaowang Lu² · Chao Yao^{1,2} · Chaoying Ni³

Received: 13 October 2015 / Accepted: 2 January 2016 / Published online: 11 January 2016
© Springer Science+Business Media New York 2016

Abstract La_{1-x}Ag_xFeO₃/halloysites nanotubes (HNTs) nanocomposite was synthesized by sol–gel method. It was characterized by X-ray diffraction, transmission electron microscope, Fourier transform infrared spectroscopy and UV–visible diffused reflectance spectroscopy measurements. The photo-activity of the La_{1-x}Ag_xFeO₃/HNTs nanocomposite was evaluated via degradation of methylene blue (MB) under visible-light irradiation. The results showed that the HNTs with unique pore structure favored the adsorption of organic molecules. Adequate Ag⁺ doping improved the absorption ability for visible light. The La_{0.95}Ag_{0.05}FeO₃/HNTs demonstrated the best photocatalytic performance, which achieved as high as 99 % for MB degradation exposed 2 h irradiation. However, further increasing of Ag⁺ doping gradually reduced the photocatalytic activity. The nanocomposite catalyst showed outstanding recyclability after eight cycles which still remained up to 90 %.

1 Introduction

Photocatalytic degradation which can take advantage of solar light and has no secondary pollution is a promising technology to deal with wastewater. In recent years, a type of inorganic compound with the defined structure of perovskite (ABO₃) in which the B cation is 6-fold coordinated, and the A cation is surrounded by an octahedron of O anions is observed to play important roles in photocatalysis application. In addition the perovskite material has high structural stability, and the A site cation can be substituted by a foreign cation having different oxidation state or radius [1], thus the content of oxygen vacancy can be tailored when desired foreign cation is used, offering a convenient and feasible way of correlating chemical properties with catalytic performances of the materials. For instance, Tijare et al. [2] synthesized nanocrystalline form (size ca. 38 nm) for photocatalytic water splitting reactions. Ma et al. [3] synthesized Mg-doped BaZrO₃ showing higher photocatalytic activity than commercial photocatalyst TiO₂. Liu et al. [4] successfully synthesized BiFeO₃–(Na_{0.5}Bi_{0.5})TiO₃ by a sol–gel method, and found that both the visible-light photocatalytic and magnetic properties were enhanced.

Although semiconductor composite particles have high photocatalytic activity, the disadvantages in terms of the separation and recycling have restricted the practical application in real condition. In recent years, carbon materials [5–7], silicon nitride composites [8], silica composites [9], zeolites composites [10] and clay minerals [11–16] have been developed as supports. More attention has been paid on the combination of semiconductor materials with different carriers to prepare supported composite photocatalyst in order to solve the above problems and reduce the cost of catalyst [17–19].

✉ Xiazhang Li
lixiazhang509@163.com

¹ Jiangsu Key Laboratory of Advanced Catalytic Materials and Technology, School of Petrochemical Engineering, Changzhou University, Changzhou 213164, People's Republic of China

² R&D Center of Xuyi Attapulgit Applied Technology, Chinese Academy of Science, Xuyi 211700, People's Republic of China

³ W.M. Keck Center for Advanced Microscopy and Microanalysis, University of Delaware, Newark, DE 19716, USA

As a clay material, halloysites (HNTs) possesses a one-dimensional tubular porous structure on the mesoporous (2–50 nm), which is larger than many synthetic porous materials such as carbon nanotube. This property enables versatile potential applications such as nanoscale support for the loading of functional nanoparticles due to its negatively charged surface [20, 21]. Moreover, HNTs has large specific surface area and pore volume, thus present strong adsorption capacity in addition to its economic viability [22, 23]. To the best of our knowledge, a successful preparation of HNTs supported perovskite nanocomposite has not yet been reported so far. In the present work, we use sol–gel method to synthesis $\text{La}_{1-x}\text{Ag}_x\text{FeO}_3$ /halloysites nanocomposite. The effect of different loading Ag^+ element on the photocatalytic activity of MB dyes was investigated.

2 Experimental

2.1 Materials and chemical

$\text{La}(\text{NO}_3)_3 \cdot 6\text{H}_2\text{O}$, $\text{C}_6\text{H}_8\text{O}_7 \cdot \text{H}_2\text{O}$, AgNO_3 , $\text{Fe}(\text{NO}_3)_3 \cdot 9\text{H}_2\text{O}$ were provided by Medicine Group Chemical Reagent Co. Ltd., Jiangsu, China. $\text{C}_{19}\text{H}_{42}\text{BrN}$ were purchased from Shanghai Ling Feng Chemical Reagent Co. Ltd. at analytical grade and used without further purification. The halloysite nanotubes were obtained from Jiangsu NDZ Technology Co. Ltd.

2.2 Synthesis of $\text{La}_{1-x}\text{Ag}_x\text{FeO}_3$ /HNTs

Adequate amount of silver nitrate, lanthanum nitrate, ferric nitrate and citric acid were mixed in 40 mL beaker under ultrasonic dissolving. The mixed solution was added by 150 mL deionized water and maintained at 90 °C for 2 h under stirring, followed by drying for 12 h at 110 °C. Subsequently, the resulting sample was milled and subject to a static thermal treatment in an oven, followed by grounded into powder with hydrochloric acid. Finally, the solution was added certain amount of halloysite by ultrasonic stirring. The composite catalyst was obtained followed by drying and calcined at 400 °C.

2.3 Characterization

The powder X-ray diffraction (PXRD) patterns were recorded with Rigaku D/MAX-2500PC diffractometer with Cu target (40 kV, 100 mA) at a scanning rate of 6 min^{-1} . TEM characterization was performed using a JEOL JEM-2100 transmission electron microscope coupled with Gatan 832 CCD and Oxford EDS operating at an accelerating voltage of 200 kV. The samples were supported on

carbon–copper grids by dropping ethanol suspensions containing uniformly dispersed oxide powders. FT-IR spectra of samples were obtained using a Nicolet 460 with diffuse reflectance sampling accessory at a resolution of 4 cm^{-1} . Measurements were performed with powders which were made using KBr powder as diluents. The UV–Vis diffuse reflectance spectra (DRS) of catalysts were recorded on a UV–Vis spectrometer (Thermo Nicolet Evolution 500) equipped with an integrating sphere.

2.4 Photocatalysis measurement

The photocatalytic activity of the samples was evaluated by photodegradation of MB under 300 W Xe lamp irradiation with a cut-off filter to remove all wavelengths lower than 420 nm. In a typical experiment, aqueous suspensions of MB (150 mL, 10 mg/L) and 0.1 g of the photocatalysts powder were placed in a quartz beaker. Prior to irradiation, the mixture was ultrasonically dispersed in the dark for 30 min to ensure the establishment of an adsorption/desorption equilibrium between the organic molecular and the surface of catalyst. At irradiation time intervals, 3 mL of the suspension was collected and centrifuged to remove the particles for analysis. The photocatalytic degradation process was monitored by measuring the absorbance at 665 nm as a function of irradiation time using a UV–Vis spectrophotometer (Spectrumlab 22 PC).

3 Results and discussion

3.1 Structural characterization

Figure 1 shows the XRD spectra of $\text{La}_{1-x}\text{Ag}_x\text{FeO}_3$ /HNTs nanocomposites with various Ag^+ doping. The $2\theta = 12^\circ$,

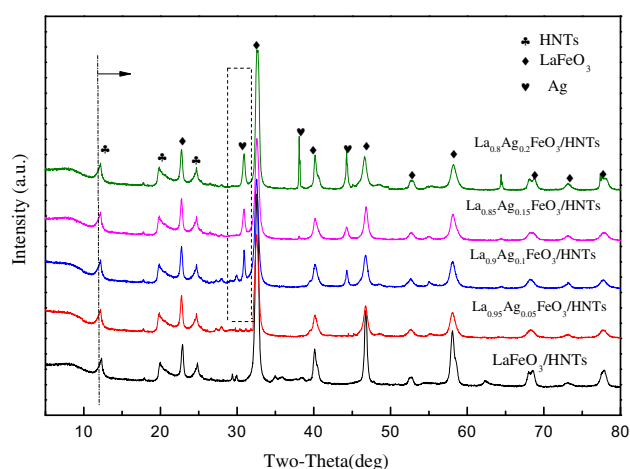


Fig. 1 XRD spectra of $\text{La}_{1-x}\text{Ag}_x\text{FeO}_3$ /HNTs with various Ag^+ doping

20° and 24° correspond to (100) (001) and (002) diffraction peaks of HNTs respectively. The $2\theta = 52^\circ, 58^\circ, 68^\circ$ and 77° are assigned to the (210), (211), (220) and (310) planes of LaFeO_3 (JCPDS 85-0987). It can be seen that the basic structure of perovskite in composite materials with different doping ratio have been maintained. With the increasing of Ag^+ doping amount, a consistent peak broadening is observed, reflecting the occurrence of more defective perovskite lattice and smaller particle size. A progressive shift of the diffraction peaks to lower Bragg angles is also observed, implying that part of Ag^+ species enters into the LaFeO_3 lattice and aggravates the expansion of its unit cell, which may be due to the substitution of La^{3+} ion (0.106 nm) by relatively larger ionic radius Ag^+ ion (0.126 nm), consequently leading to lattice distortion as well as the formation of more oxygen vacancies, both of which may enhance the photocatalytic capability of the nanocomposites [24]. It is noticed that the (100) peak of HNTs slightly shifts to higher Bragg angle as well, which can be attributed to the incorporation of O^{2-} from LaFeO_3 into the HNTs support, resulting in the shrinkage of the basal distance of the HNTs suggesting that $\text{La}_{1-x}\text{Ag}_x\text{FeO}_3$ has been successfully loaded onto the HNTs surface. It is worth mentioning that the characteristic diffraction peak at 32° and 44° corresponding to Ag (JCPDS 87-0597) appears and enhances when the Ag^+ doping ratio is 0.1 or beyond, suggesting the co-precipitation of Ag species.

Figure 2 shows the TEM images of $\text{LaFeO}_3/\text{HNTs}$ samples with different loading amount of LaFeO_3 . Figure 2a shows the pure LaFeO_3 , it can be seen that there is an obvious aggregation of particles. Figure 2b shows that the halloysite appears as 1-D tubular structure with uniform diameters ranging from 30 to 50 nm and lengths ranging from 0.5 to 1 μm . As can be seen in Fig. 2c, The LaFeO_3 nanoparticles with average diameter of 20 nm, together with small clusters of the LaFeO_3 nanoparticles, evenly coat the surface of HNTs when the weight percentage is relatively low. With gradual increase of LaFeO_3 , the number of LaFeO_3 nanoparticles increases as well. When the loading amount is 20 wt% (Fig. 2d), the LaFeO_3 nanoparticles are uniformly dispersed on the surface of HNTs with the absence of obvious agglomerating and few nanoparticles are observed to be detached from the surface of the nanotubes. However, as the loading amount increase to 30 wt% (Fig. 2e), the size of nanoparticles on the surface of HNTs gradually increase accompanied with the aggravation of agglomeration. Apparent aggregation of LaFeO_3 particles on the outside of the HNTs appears when the LaFeO_3 content reaches 40 % (Fig. 2f). The results also suggest that as the mass ratio of LaFeO_3 increases, the phase evolution does not significantly change the general morphology of the HNTs, adequate amount of LaFeO_3 can maintain a well-defined structure to achieve excellent

immobilization of the nanoparticles. When loading amount is higher than 20 wt%, however, the abnormal precipitation and over-growth of LaFeO_3 particles eventually lead to the appearance of obvious agglomeration of loaded perovskite particles. Therefore, the optimal loading amount is determined to be 20 wt%.

The UV–Vis spectra of $\text{LaFeO}_3/\text{HNTs}$ and $\text{La}_{0.95}\text{Ag}_{0.05}\text{FeO}_3/\text{HNTs}$ are shown in Fig. 3 respectively. It can be seen that an adsorption band in the ultraviolet range of 400–650 nm appears for $\text{LaFeO}_3/\text{HNTs}$ nanocomposites in Fig. 3a, representing the characteristics of loading LaFeO_3 . However in Fig. 3b, a new strong adsorption band in the visible range of 400–750 nm in addition to the reduced adsorption edge of $\text{La}_{0.95}\text{Ag}_{0.05}\text{FeO}_3/\text{HNTs}$ appear, which may be ascribed to the visible adsorption of Ag^+ doping [25]. The results show that the $\text{La}_{0.95}\text{Ag}_{0.05}\text{FeO}_3/\text{HNTs}$ exhibits enhanced visible-light adsorption which promises an opportunity for the utilization of visible light, a major component of sunlight.

Figure 4 shows the FT-IR spectra of HNTs, $\text{La}_{0.95}\text{Ag}_{0.05}\text{FeO}_3$ and $\text{La}_{0.95}\text{Ag}_{0.05}\text{FeO}_3/\text{HNTs}$. The two peaks between 3410 and 3493 cm^{-1} are ascribed to hydroxyl stretching vibration in the HNTs surface. The absorption peak of 1623 cm^{-1} is attributed to the bending vibration of the surface adsorbed water and the H–O–H bond of the interlayer water molecules. Absorption peak at 567 cm^{-1} is assigned to the stretching and bending vibration of Fe–O bond in the perovskite lattice. Absorption peak of Ag–O bond stretching vibration and bending vibration of the absorption peak should appear at around 1350 cm^{-1} , however the peak intensity is very weak due to the low doping amount of Ag^+ . The intensity of $\text{La}_{0.95}\text{Ag}_{0.05}\text{FeO}_3/\text{HNTs}$ tends to be weaker near the absorption peak between 3465 cm^{-1} and 1020 cm^{-1} in HNTs. This may be due to the dispersion of $\text{La}_{0.95}\text{Ag}_{0.05}\text{FeO}_3$ on the HNTs surface.

3.2 Catalytic property

The photocatalytic activity of nanocomposite is examined using visible light for MB degradation as shown in Fig. 5. After reaching adsorption/desorption equilibrium in 30 min, the order of adsorption rate for MB is as follows: $\text{La}_{1-x}\text{Ag}_x\text{FeO}_3/\text{HNTs} > \text{La}_{1-x}\text{Ag}_x\text{FeO}_3 > \text{LaFeO}_3/\text{HNTs} > \text{LaFeO}_3 > \text{HNTs}$, indicating that the Ag^+ incorporation has a conducive effect on adsorption rate for MB. The concentration of MB has barely changed after 30 min when HNTs is used as catalyst, indicating that HNTs has no photocatalytic activity. The rate reaches a maximum of only 10 % solely due to the adsorption of MB on the surface of HNTs. The reaction may happen between the hydroxyl groups of the HNTs and the cationic group in the dye molecules favoring the interaction and adsorption [26]. In decomposition experiments under visible light

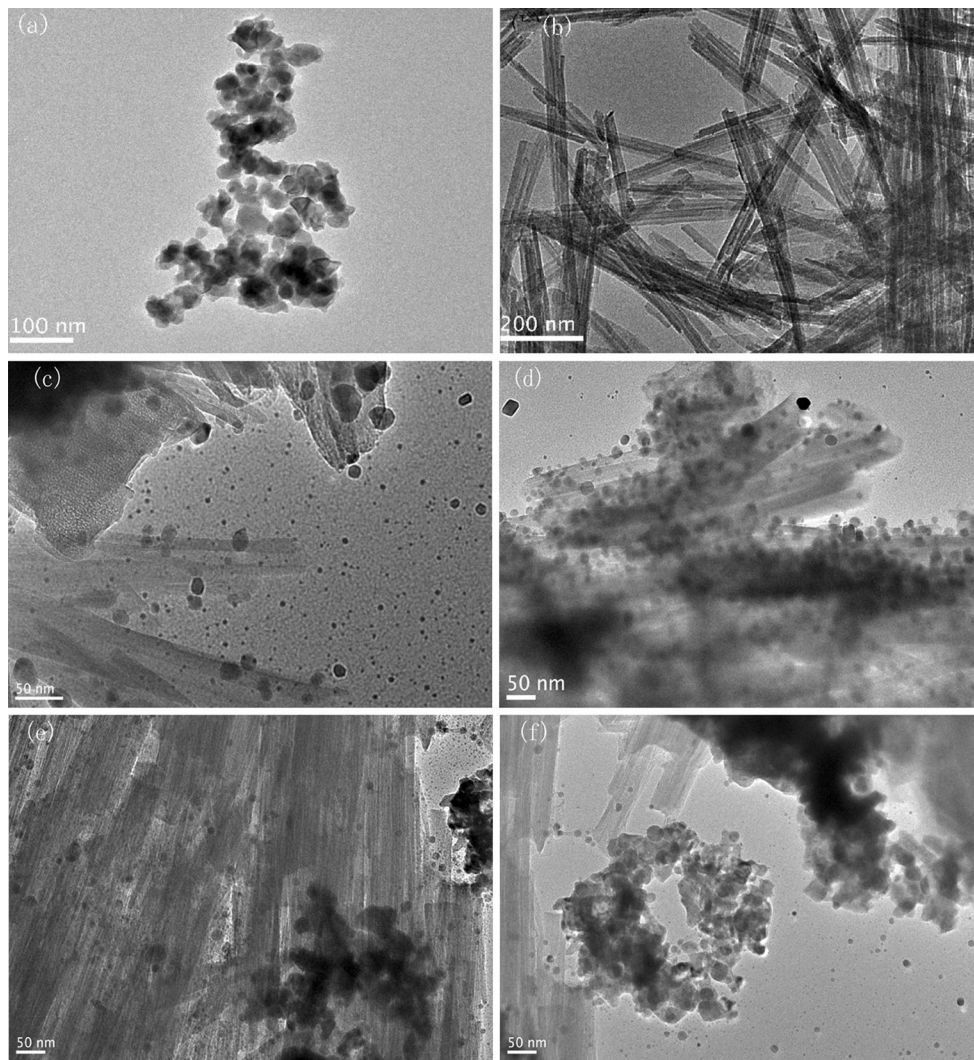


Fig. 2 TEM of HNTs and LaFeO₃/HNTs samples with various loading amount **a** LaFeO₃, **b** HNTs, **c** 10 wt%, **d** 20 wt%, **e** 30 wt%, **f** 40 wt%

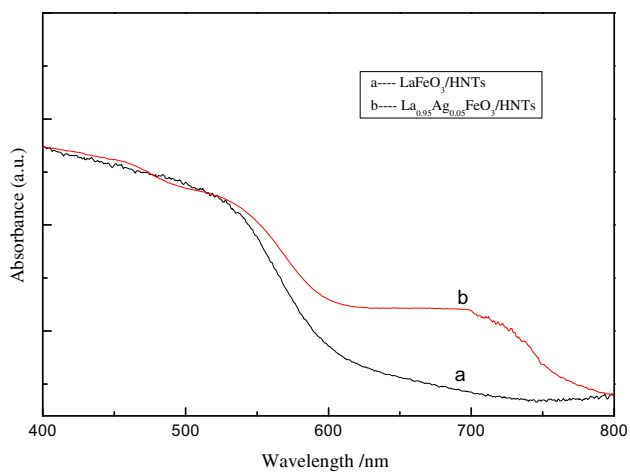


Fig. 3 UV-Vis diffuse reflectance spectra of the composite catalyst **a** LaFeO₃/HNTs, **b** La_{0.95}Ag_{0.05}FeO₃/HNTs

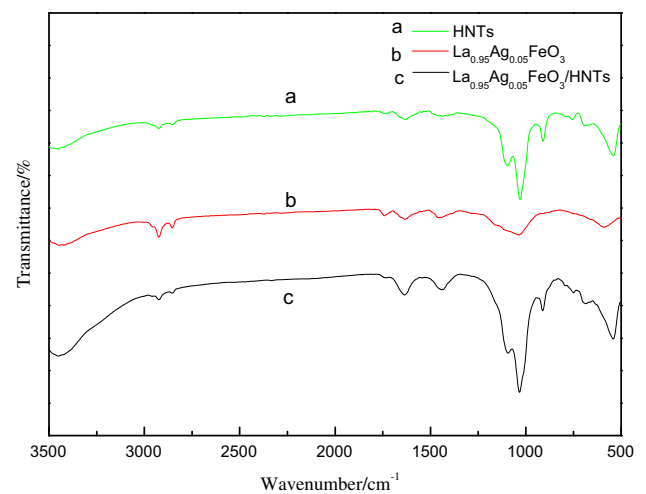


Fig. 4 FT-IR spectra of different samples **a** HNTs, **b** La_{0.95}Ag_{0.05}FeO₃, **c** La_{0.95}Ag_{0.05}FeO₃/HNTs

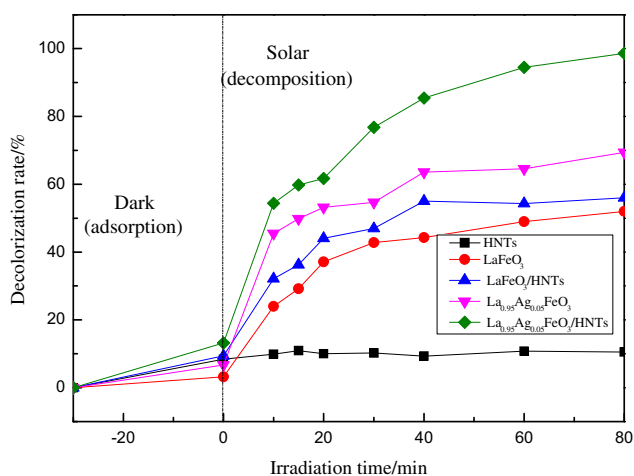


Fig. 5 Photocatalytic degradation of MB in aqueous under visible light irradiation

irradiation with $\text{LaFeO}_3/\text{HNTs}$ catalyst, the degradation of MB increase up to 47 % and remains almost unchanged as a function of radiation time, thereby demonstrating that $\text{LaFeO}_3/\text{HNTs}$ is not an active photocatalyst. However, the conversion for $\text{La}_{0.95}\text{Ag}_{0.05}\text{FeO}_3/\text{HNTs}$ increase significantly up to 99 %, as compared with the 62 % rate when $\text{La}_{0.95}\text{Ag}_{0.05}\text{FeO}_3$ is used, indicating that the nanocomposite has remarkable photocatalytic activity which is attributed to the Ag^+ doping increasing the visible light absorption, as well as the contribution of HNTs support.

Figure 6 shows the effect of molar fractions on the photocatalytic degradation of MB under visible light irradiation. A remarkable increase for up to 99 % is observed when the molar fraction of Ag^+ is 0.05 compared to no doping. This may be due to the fact that Ag^+ doping improves the adsorption of visible light and lower the band

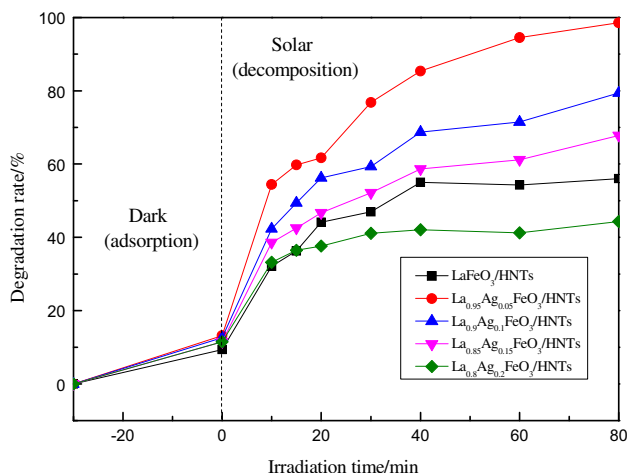


Fig. 6 Effect of molar fraction of Ag^+ on the degradation rate of MB under visible light irradiation

gap (E_g) of the perovskite as evidenced by UV–Vis measurement. However, the product shows lower conversion when the Ag^+ amount is increased above 0.05, and even lower when Ag^+ is 0.2 showing a conversion of 38 %. It can be rationalized that the co-precipitated Ag species as identified in XRD results may prevent the utilization of visible light. Therefore, 0.05 appears to be an optimal molar fraction of Ag^+ for the nanocomposite catalyst.

The repeated MB bleaching experiment on $\text{La}_{0.95}\text{Ag}_{0.05}\text{FeO}_3/\text{HNTs}$ is examined in Fig. 7. After eight consecutive runs, the bleaching rate is slightly decreased, and the conversion of MB maintains as high as 90 %, indicating an outstanding recyclability under visible light. Compared with $\text{La}_{0.95}\text{Ag}_{0.05}\text{FeO}_3$ catalyst, the enhanced dispersion of nanoparticles on support as well as remarkable adsorption capability of HNTs, consequently improves the interacting area between active sites and dye molecules. Moreover, both $\text{La}_{0.95}\text{Ag}_{0.05}\text{FeO}_3/\text{HNTs}$ and $\text{La}_{0.95}\text{Ag}_{0.05}\text{FeO}_3$ catalyst have been characterized by TEM (not shown here) after the photo-degradation reaction. There are no appreciable morphological changes observed for $\text{La}_{0.95}\text{Ag}_{0.05}\text{FeO}_3/\text{HNTs}$. However, abnormal particle growth is found to contribute to the deactivation of the unsupported $\text{La}_{0.95}\text{Ag}_{0.05}\text{FeO}_3$, further implying that HNTs plays a significant role in the immobilization of the active particles.

According to the above results, a plausible photocatalysis mechanism is proposed and elucidated schematically in Fig. 8. Under visible light irradiation, the electrons (e^-) in full valence band of perovskite can move to the empty conduction band, thus leaving an equivalent number of holes (h^+) with positive charge in corresponding positions [27]. On one hand, the presence of Ag^+ doping favors the utilization of visible light region, moreover when the La^{3+}

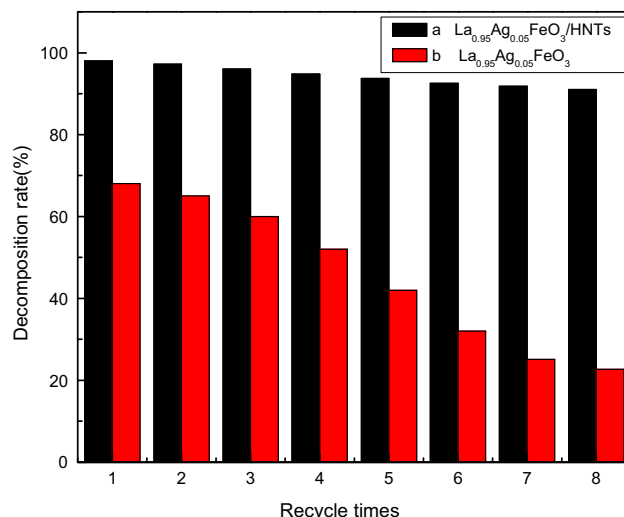


Fig. 7 Effect of recycle time on the decomposition rate of MB, a $\text{La}_{0.95}\text{Ag}_{0.05}\text{FeO}_3/\text{HNTs}$, b $\text{La}_{0.95}\text{Ag}_{0.05}\text{FeO}_3$

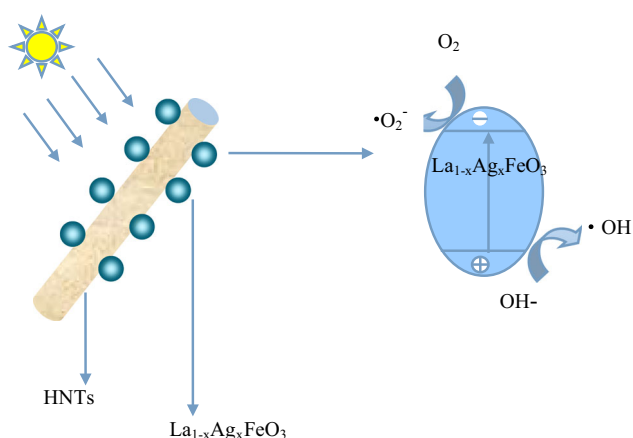


Fig. 8 Photocatalytic mechanism of $\text{La}_{1-x}\text{Ag}_x\text{FeO}_3/\text{HNTs}$ nanocomposite

is substituted by Ag^+ , the local charge turns to be imbalance leading to mixed state (Fe^{3+} and Fe^{4+}), in which Fe^{3+} acts as electron trap thus retards the recombination of electrons and holes. The electrons and holes will then react with oxygen molecules and ions in solution to finally form superoxide radical O_2^- and hydroxyl radicals $\cdot\text{OH}$ respectively. These radicals will further decompose the MB molecules which are preferentially adsorbed onto the HNTs surface due to the fact that the presence of surface hydroxyl groups have Van der Waals and hydrogen bonding interaction with dye molecules though the binding is weak [28]. Nonetheless, further research should shed light on the above preliminary mechanism proposed for this novel nanocomposite.

4 Conclusions

In conclusion, $\text{La}_{1-x}\text{Ag}_x\text{FeO}_3/\text{HNTs}$ nanocomposite has been successfully prepared. The doping of Ag^+ broadens the visible light absorption range of perovskite and improves the catalytic performance of the catalyst. The degradation efficiency of MB is the best which reaches as high as 99 % when $x = 0.05$. With further increase of Ag^+ doping ratio, the degradation rate of MB gradually decreases. Experiments prove that the $\text{La}_{1-x}\text{Ag}_x\text{FeO}_3/\text{HNTs}$ nanocomposite photocatalyst can be used repeatedly for eight runs without significant rate reduction. The adsorptive capability of HNTs and the enhanced electron transferring in $\text{La}_{1-x}\text{Ag}_x\text{FeO}_3$ compound are both in favor of the photocatalytic performance.

Acknowledgments This work was partially supported by the National Science Foundation of China (51002016), Priority Academic Program Development of Jiangsu Higher Education Institutions

(PAPD), Jiangsu Technology Support Program (BE2014100, BE2014103), Jiangsu International Cooperation Project (BZ2015040) and Huai'an International Cooperation Project (HAC2014014).

References

- M.A. Bhat, A. Modi, N.K. Gaur, *J. Mater. Sci. Mater. Electron.* **26**, 6444 (2015)
- S.N. Tijare, M.V. Joshi, P.S. Padole, P.A. Mangrulkar, S.S. Rayalu, N.K. Labhsetwar, *Int. J. Hydrogen Energy* **37**, 10451 (2012)
- X.L. Ma, J.C. Zhang, *J. Alloys Compd.* **580**, 664 (2013)
- H.Y. Liu, Y.P. Guo, B. Guo, *Solid State Sci.* **6**, 7216 (2012)
- Y. Ma, Y. Chen, *Natl. Sci. Rev.* **2**, 40 (2015)
- Z.Z. Jiang, Z.B. Wang, Y.Y. Chu, D.M. Gu, G.P. Yin, *Energy Environ. Sci.* **4**, 2558 (2011)
- T.Y. Peng, P. Zeng, D.N. Ke, X.J. Liu, X.H. Zhang, *Energy Fuels* **25**, 2203 (2011)
- H. Yamashita, H. Nose, Y. Kuwahara, Y. Nishida, S. Yuan, K. Mori, *Appl. Catal. A* **350**, 164 (2008)
- Q. Zhang, J. Liu, Y. Cui, W. Ding, *J. Mater. Sci. Mater. Electron.* **26**, 3291 (2015)
- G. Nabyouni, A. Shabani, S. Karimzadeh, J. Ghasemi, H. Ramazani, *J. Mater. Sci. Mater. Electron.* **26**, 5677 (2015)
- R.J. Tayade, R.G. Kulkarni, R.V. Jasra, *Ind. Eng. Chem. Res.* **46**, 369 (2007)
- G. Varadwaj, S. Rana, K. Parida, B.B. Nayak, *J. Mater. Chem. A* **2**, 7526 (2014)
- G.K. Zhang, X.M. Ding, F.S. He, X.Y. Yu, J. Zhou, Y.J. Hu, J.W. Xie, *Langmuir* **24**, 1026 (2008)
- G. Zhang, Y. Gao, Y. Zhang, Y. Guo, *Environ. Sci. Technol.* **44**, 6384 (2010)
- P. Aranda, R. Kun, M.A. Martín-Luengo, S. Letaïef, I. Dékány, E. Ruizhitzky, *Chem. Mater.* **20**, 84 (2008)
- A. Rodríguez, G. Ovejero, M. Mestanza, J. García, *Ind. Eng. Chem. Res.* **49**, 3207 (2010)
- D. Han, J. Cao, S. Yang, J. Yang, B. Wang, Q. Liu, T. Wang, H. Niu, *J. Mater. Sci. Mater. Electron.* **26**, 7415 (2015)
- J.H. Zhang, L.L. Zhang, J.S. Lv, S.Y. Zhou, H.Q. Chen, Y.J. Zhao, X. Wang, *Appl. Clay Sci.* **90**, 135 (2014)
- Y.M. Hunge, V.S. Mohite, S.S. Kumbhar, K.Y. Rajpure, A.V. Moholkar, C.H. Bhosale, *J. Mater. Sci. Mater. Electron.* **26**, 8404 (2015)
- M. Kitano, M. Hara, *J. Mater. Chem.* **20**, 627 (2010)
- M.N. Chong, B. Jin, C.W.K. Chow, C. Saint, *Water Res.* **44**, 2997 (2010)
- V.S. Reddy, S.C. Kaushik, K.R. Ranjan, S.K. Tyagi, *Renew. Sustain. Energy Rev.* **27**, 258 (2013)
- M. Ni, M.K.H. Leung, D.Y.C. Leung, K. Sumathy, *Renew. Sustain. Energy Rev.* **11**, 401 (2007)
- X.Z. Li, C.Y. Ni, C. Yao, Z.G. Chen, *Appl. Catal. B* **117**, 118 (2012)
- N. Labhsetwar, G. Saravanan, S. Megarajan, N. Manwar, R. Khobragade, P. Doggali, F. Grasset, *Sci. Technol. Adv. Mater.* **16**, 1 (2015)
- P. Yuan, D. Tan, F. Annabi-Bergaya, *Appl. Clay Sci.* **112**, 75 (2015)
- M.H.S. Abhudhahir, J. Kandasamy, *J. Mater. Sci. Mater. Electron.* **26**, 8307 (2015)
- X.Z. Li, C. Yao, X.W. Lu, Z.L. Hu, Y. Yin, C.Y. Ni, *Appl. Clay Sci.* **104**, 74 (2015)